

Poly(styrene/pentafluorostyrene)-block-Poly(vinyl alcohol/vinylpyrrolidone) Amphiphilic Block Copolymers for Kinetic Gas Hydrate Inhibitors: Synthesis, Micellization Behaviour, and Methane Hydrate Kinetic Inhibition.

Faraz Rajput, Antonio Colantuoni, Salim Bayahya, Riadh Dhane, Phillip Servio, Milan Maric

Department of Chemical Engineering, McGill University, 3610 University Street, Montreal, Quebec, Canada, H3A 0C5

Correspondence to: Milan Maric (E-mail: milan.maric@mail.mcgill.ca)

ABSTRACT

Amphiphilic block copolymers of short poly(styrene) (PS) or poly(2,3,4,5,6-pentafluorostyrene) (PPFS) segments with comparatively longer poly(vinyl acetate) (PVAc) or poly(vinylpyrrolidone) (PVP) segments are synthesized using a 2-cyanopropan-2-yl N-methyl-N-(pyridin-4-yl)dithiocarbamate switchable RAFT agent towards application as kinetic gas hydrate inhibitors (KHI). Polymerization conditions are optimized to provide water-soluble block copolymers by first polymerizing more activated monomers (MAM) such as S and PFS to form a defined macro chain-transfer agent (linear degree of polymerization with conversion, comparatively low dispersity) followed by chain extensions with less activated monomers (LAM) VAc or VP by switching to the deprotonated form of the RAFT agent. The critical micelle concentrations (CMCs) of these amphiphilic block copolymers (after VAc unit hydrolysis to vinyl alcohol units) are measured using zeta surface potential measurements to estimate physical behavior once mixed with the hydrates. A PS-PVA block copolymer improved inhibition to 49% compared to the pure methane-water system with no KHIs. This inhibition was further reduced by 27% by substituting the PS with a more hydrophobic PPFS. A block copolymer of PS-PVP exhibited 20% greater inhibition than the PVP homopolymer and substitution PS with a more hydrophobic PPFS resulted in a 35% further decreased in methane kinetic hydrate inhibition.

KEYWORDS: Amphiphilic block copolymer, switchable RAFT agent, kinetic hydrate inhibitors

INTRODUCTION

Gas hydrates are crystalline structures where water forms a cage structure around a guest gas molecule. In gas hydrates, the cage network is formed by water molecules that are linked together by strong hydrogen bonds while the guest gas molecules further stabilize the structure with van der Waals forces.¹ When appropriate conditions for the formation of gas hydrates are met, the formation of gas hydrates, depending on their

location, can be problematic. For instance, the formation of hydrates in gas pipelines may hinder the flow by forming plugs throughout.² These hydrate plugs can damage the pipelines as well as the equipment in the process downstream and can lead to environmental disasters.³ Thermodynamic gas hydrate inhibitors, such as methanol and ethylene glycol, are often added to these systems to prevent hydrate formation.⁴ Due to the large quantities of these alcohols and electrolytes required, and increased cost of thermodynamic inhibition, increasing

interest is going towards the development of kinetic hydrate inhibitors (KHIs) as substitutes to thermodynamic inhibitors.⁵ KHIs are compounds which delay the onset of nucleation and slow the growth rate of hydrate crystals.⁶ They are required in much lower quantities (<1 wt%) within the flow and greatly lower the costs for inhibition.⁵

To be effective, KHIs require high solubility in water as well as the ability to adsorb well to the polar surface of hydrate crystals.^{7,8} The effectiveness of KHIs can further increase if these polymers have hydrophobic properties.⁹ The requirement of these properties has led to the use of vinyl-based polymers, such as poly(N-vinylpyrrolidone) (PVP) and poly(N-vinylcaprolactam) (PVCap), with functional groups having large tendencies for hydrogen bonding.¹⁰ However, most of the studies currently looking at polymers as kinetic hydrate inhibitors focus on using homopolymers^{7,11} or statistical copolymers¹² and have shown vinyl esters or lactams to be effective inhibitor monomers in polymers for KHIs. Furthermore, it has been proven very difficult to understand the exact mechanism¹³ of kinetic inhibitions. One of the commonly accepted mechanisms for kinetic inhibition hypothesized that kinetic hydrate inhibitors inhibit hydrate formation by adsorbing onto the growing crystal surface through hydrogen bonds and greatly reduce the surface area available to water to go in to the hydrate phase.¹¹ Block copolymers with pronounced amphiphilic properties and controlled microstructures have not been widely studied as KHIs despite their structure being highly advantageous.^{14,15} Such segmented amphiphilic block copolymers are expected to adsorb onto the growing crystal surface of clathrate hydrates and delay this growth process, as they inherently have a hydrophilic segment to be soluble in the ice/water phase

but have a hydrophobic segment that is compatible with the gases forming hydrate.⁷

Traditionally, the synthesis of such AB amphiphilic block copolymers has only been possible via living polymerization methods (eg. ionic since the 1950s¹⁵, group transfer polymerization later in the 1980s¹⁷) to impart precise control of the segment length and ultimately composition. These techniques have been the most widely-accepted polymerization methods for academic study as properties could be easily correlated to the structure. However, such living methods require rigorous purification of monomers and solvents, pyrophoric initiators often, and completely air and moisture-free transfers.^{18,19} To combat some of these drawbacks, methods involving stable radicals, such as nitroxide mediated polymerization (NMP), atom transfer radical polymerization (ATRP), and reversible addition-fragmentation chain transfer (RAFT) polymerization, began emerging in the late 1980s and early 1990s.^{20,21,22,23} RAFT in particular is quite versatile, as it can polymerize a wide range of monomers and depending on the choice of the thiocarbonyl compound as the chain transfer agent, it can polymerize styrenics, methacrylates, acrylamides (more activated monomers, MAM) as well as vinyl esters (less activated monomers, LAM).^{24,25} During RAFT polymerization, these chain transfer agents establish an equilibrium with the dormant chains and propagating radicals.²⁴ This equilibrium provides equal probability for all chains to grow simultaneously.²¹ Once the reaction is stopped, the polymer chains retain the thiocarbonyl group from the RAFT agent and may act as a macro RAFT chain-transfer agent (CTA) to chain-extend with another batch of monomer, thereby producing block copolymers.²⁶ One of the major drawbacks of synthesizing block co-polymers using RAFT is that the CTAs suitable for

polymerization of MAMs are often ineffective with LAMs and vice versa, making it difficult to combine these two monomer types into a single block copolymer.

To overcome this drawback, increasing interest is going towards a new class of stimuli responsive or “switchable”, dithiocarbamate and trithiocarbonate based RAFT agents.^{27,28} These RAFT agents are effective in polymerizing MAMs as well as LAMs depending on whether it is in its protonated or “switched” deprotonated form. Recently, switchable RAFT agents, such as 2-cyanopropan-2-yl *N*-methyl-*N*-(pyridin-4-yl)dithiocarbamate, have been reported to offer good control over the polymerization of MAMs including styrene as well as vinyl based LAMs.²⁹ Figure 1 shows the reaction

scheme used in this study to form amphiphilic block copolymers as KHIs.

LAMs, such as VAc and VP, are particularly desirable in kinetic hydrate inhibitors as they inhibit hydrate formation and growth by adsorbing onto them. Additionally, to study the self-assembly process of block copolymers in KHIs and the effect of the hydrophobic, gas-soluble segment, these block copolymers require acrylate/methacrylate or styrenic-based polymer end groups, which are MAMs. Therefore, switchable RAFT agents present themselves as promising candidates in the synthesis of these LAM-MAM block copolymers for KHIs.

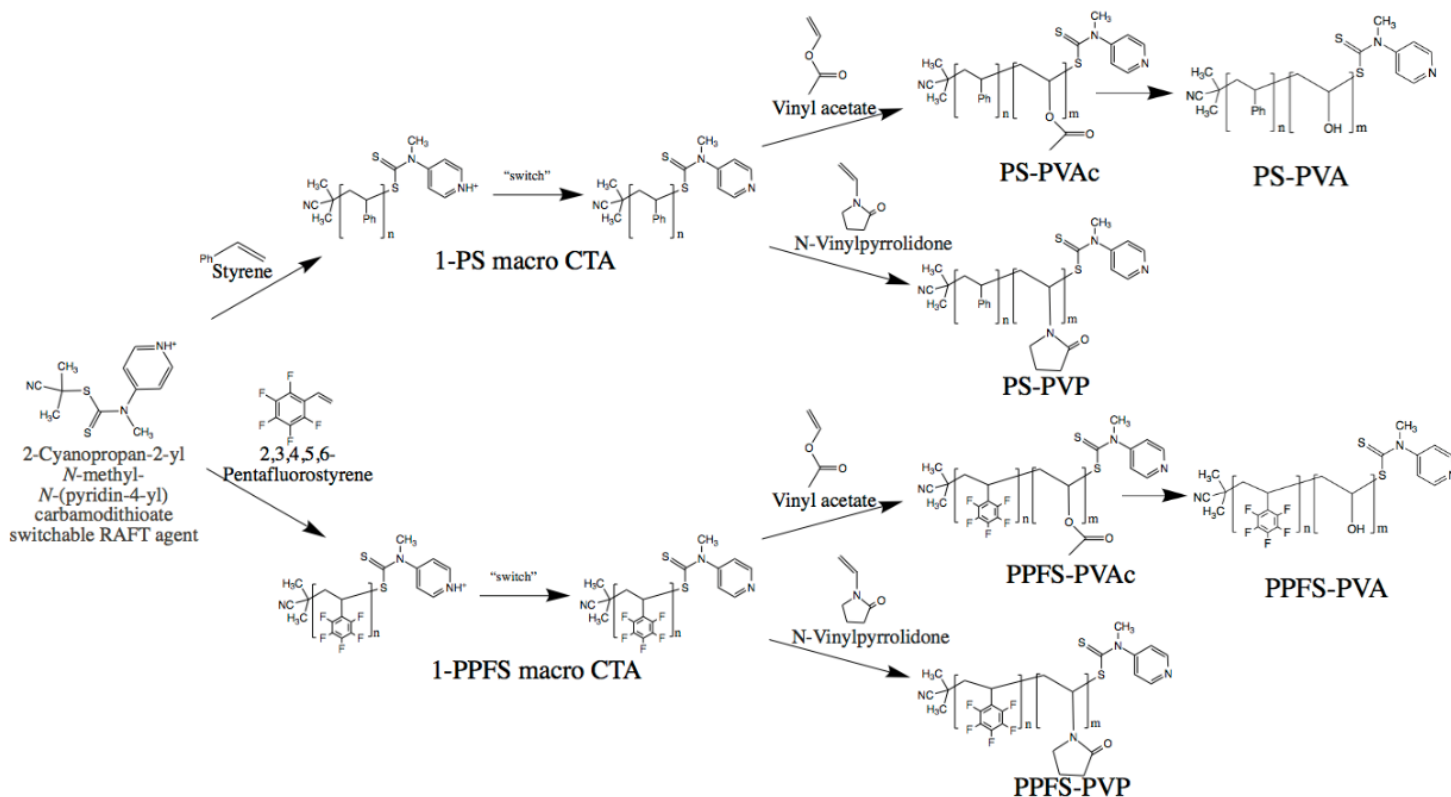


Figure 1: Reaction scheme for synthesizing LAM-block-MAM copolymers used as KHIs. Styrene or 2,3,4,5,6-pentafluorostyrene is synthesized with a switchable RAFT agent to form a macro CTA. The macro CTA is “switched” to its deprotonated form before being chain extended with vinyl acetate or vinylpyrrolidone to form an amphiphilic block copolymer KHI. Vinyl acetate units in the PS-PVAc and the PPFS-PVAc block copolymers were converted to vinyl alcohol (VOH) to give the water-soluble block copolymers PS-PVOH and PPFS-PVOH, respectively

Critical micelle concentration

A simple method to determine the CMC has recently been reported, whereby the surface (zeta potential) charge of the block copolymer in solution can be correlated with CMC.³⁰ This surface charge is expected to decrease with increasing concentrations until all polymers have formed micelles (CMC) and the surface charge plateaus.^{12,31,30} This method has been used mostly with small surfactants but has not been applied with large molecular weight amphiphilic block copolymers.

This study aims at synthesizing block copolymers of poly(N-vinyl alcohol) (PVA) or PVP with poly(styrene) (PS) or poly(pentafluorostyrene) (PPFS) to form KHIs with more pronounced amphiphilic properties. For this purpose, a newer, more simplified, RAFT synthesis procedure, compared to traditional RAFT procedures involving multiple RAFT agents and purification steps, using a “switchable” RAFT agent is being investigated.

The effectiveness of these block copolymers in inhibiting methane hydrate growth is also investigated.

EXPERIMENTAL SECTION

Materials

2-Cyanopropan-2-yl N-methyl-N-(pyridin-4-yl) carbamodithioate (switchable RAFT agent, >97%, Sigma-Aldrich), azobis isobutyryl nitrile (AIBN), N,N-dimethylformamide (DMF, >95%, certified ACS, Acros Organics), vinyl acetate (VAc monomer, >99%, contains 3-20 ppm

hydroquinone inhibitor, Sigma-Aldrich), 2,3,4,5,6-pentafluorostyrene (PFS monomer, 99%, contains 0.1% inhibitor, Sigma-Aldrich), styrene (S monomer, 99.9%, ReagentPlus, Sigma-Aldrich), 1-vinyl-2-pyrrolidinone (VP monomer, >97.0%, purum, Sigma-Aldrich), tetrahydrofuran (THF, >99.9%, HPLC grade, Fisher Scientific), reverse osmosis (RO) purified H₂O, were used as received, trifluoromethanesulfonic acid (>99%, ReagentPlus, Sigma-Aldrich). The methane gas used for hydrate growth experiments was obtained from MEGS Inc. with ultra-high purity in excess of 99.99%.

Sample preparation for synthesis of macro chain-transfer agents

The synthesis of 1-poly(styrene) (1-PS) and 1-poly(2,3,4,5,6-pentafluorostyrene) (1-PPFS) macro chain-transfer agents were conducted at 70 °C for a duration of 360 mins. For these polymerizations, a solution containing 10.00 g of the desired monomer (S or PFS at 0.1 mol and 0.05 mol respectively), 0.01 mole equivalents of 2-cyanopropan-2-yl N-methyl-N-(pyridin-4-yl)dithiocarbamate switchable RAFT agent, 0.002 mole equivalents of AIBN initiator, and 0.01 mole equivalents of trifluoromethanesulfonic acid was prepared in a round bottom flask. The reactants were degassed with at least 3 freeze-pump-thaw cycles. The macro-chain transfer agents were synthesized to 45% and 51% conversions (for 1-PS and 1-PPFS respectively) and are shown in Table 1. These macro CTAs were used for chain extensions.

Table 1: Experimental reaction conditions for chain extension polymerization reactions of 1-PS and 1-PPFS with VAc and VP.

Experiment ID	Macro chain-transfer agent ^a (Mn [kg mol ⁻¹], <i>D</i>)	Monomer ^b	Reaction Temperature	Reaction Duration (hr)	Target MW ^c M _{n,th} (kg mol ⁻¹)
PS-PVAc	1-PS (4.2, 1.38)	VAc	70 °C	19	100
PS-PVP	1-PS (2.2, 1.41)	VP	70 °C	3	100
PPFS-PVAc	1-PPFS (4.8, 1.35)	VAc	70 °C	19	100
PPFS-PVP	1-PPFS (2.6, 1.42)	VP	70 °C	3	100

^aThe first term indicates the macro chain-transfer agent used to initiate the second batch of monomer. Mn and *D* (values in parenthesis) represent the number average molecular weight of the previously synthesized macro chain-transfer agents used to chain extend and form a block copolymer as well as its dispersity. ^b The monomer with which the macro chain-transfer agent was chain extended. ^c The target molecular weight (MW) represented the molecular weight of the polymer expected to achieve at 100% conversion of the monomer.

Sample preparation for chain extension

For the chain extension reactions, solutions containing 10.00 g of the desired monomer for extension (VAc, or VP at 0.1 mol), 5×10^{-4} equivalent moles of the macro chain-transfer agent (1-PS or 1-PPFS), and 0.001 equivalent moles of AIBN initiator was prepared in a round bottom flask. The reactants were degassed with at least 3 freeze-pump-thaw cycles. Chain extension polymerization reactions were conducted at 70 °C. A summary of the reaction conditions is presented in Table 1.

Freeze-pump-thaw

Prior to beginning a reaction, air is removed from the reactants mixture through freeze-pump-thaw cycles. A Schlenk line was setup for the removal of air from the solutions. A Chemglass air-free Schlenk tube was held in place by support stands. The vacuum tube of the Schlenk line was connected to a vacuum pump. The atmospheric tube of the Schlenk line was connected to the nitrogen gas tank purchased from MEGS Specialty Gases and

Equipment Inc. while the other end of the Schlenk line was open to the atmosphere. The Schlenk line system was connected to a Chemglass air-free 100 mL, 24/40, round bottom flask in which the solution to be degassed would be placed. The flask was mounted on the support stand and a jack held a dewar flask, containing liquid nitrogen, underneath the round bottom flask for the freezing step.

Polymerization

All polymerization reactions were performed in a Dima Glass 50 mL round bottom flask with three 24/40 fitting necks, placed in a heating mantle. A 50 mL three-neck round bottom flask reactor was placed on the heating mantle on the magnetic stirrer. The reactor was connected by the middle neck to the condenser column through which the cooling liquid was circulating. A small magnetic stir bar was added to the reactor and the remaining two necks of the reactor were shut using rubber septa. A thermocouple was inserted into the reactor through the septa. A nitrogen gas purge line needle was also

inserted in the reactor from the septum of the third neck. The reactor was purged for 20 minutes to ensure an oxygen free environment.

Following the completion of the purging cycle, the reactant sample solution, prepared and degassed earlier, was added to the reactor using a syringe. After the addition of the reactant solution, the reactor was further purged for 5 minutes using nitrogen gas to remove any air that might have entered the reactor during the addition of the reactant solution. Following the second purge cycle, the temperature controller and the heating mantle were turned on to increase the temperature to the experimental temperature (listed in Table 1) and allow for the polymerization reaction to begin. The reactions were run for a set time duration as given in Table 1. The synthesized block copolymers were purified by dissolving in tetrahydrofuran and precipitating in heptane.

Characterization

Gel permeation chromatography

The number-average molecular weight (M_n) and dispersity (\mathcal{D}) of the obtained polymers were measured using gel permeation chromatography. The GPC was equipped with three Styragel® HR columns (HR1, HR2, and HR3) with molecular weight measurement ranges from 0.1 kg mol⁻¹ to 5 kg mol⁻¹, 0.5 kg mol⁻¹ to 20 kg mol⁻¹, and 5 kg mol⁻¹ to 500 kg mol⁻¹, respectively. The mobile phase used in these columns was HPLC grade THF, with a flow rate of 0.3 mL min⁻¹. Poly(methyl methacrylate) (PMMA), having molecular weight range from 1 kg mol⁻¹ to 1677 kg mol⁻¹, was used as standards for the calibration. The differential refractive index (RI 2410) detector was used for the measurements.

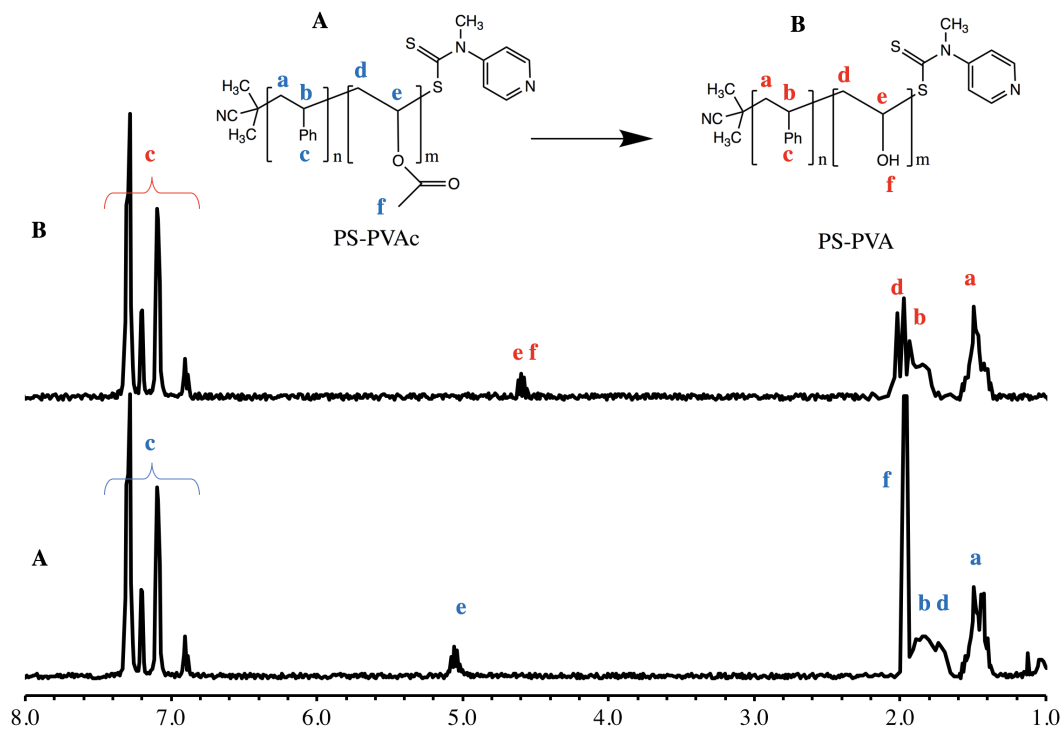


Figure 2: ¹H NMR (CDCl₃) of PS-PVAc block copolymer: A) before hydrolysis and B) after treatment with NaOH to yield water-soluble PS-PVOH block copolymer.

¹H-NMR

The conversion of the various samples taken throughout the reactions was determined using NMR. ¹H-NMR measurements were performed in deuterated dimethyl sulfoxide (DMSO) solvent with a 500 MHz Varian Mercury NMR. The conversions of S, PFS, VAc, and VP were determined by looking at the ratio of the area associated with the vinylic protons in the monomer disappearing, relative to the rest of the protons in the monomer, as the reactions progressed.

CMC measurements

Varying concentrations (100 ppm, 200 ppm, 400 ppm, 800 ppm, 1600 ppm, 3200 ppm, 7000 ppm, 14000 ppm, 28000 ppm, and

56000 ppm) of the synthesized polymers were prepared. Block copolymers were weighed and added to deionized water at room temperature to make the highest concentration of polymer solution first. No buffer was added to the mixture. This solution was then dissolved in water to achieve lower concentration. 1 mL of the polymer solution was placed in a disposable capillary cell which was inserted into the ZetaSizer. The surface (zeta potential) charge was measured using the ZetaSizer Nano ZS by Malvern. The Zetasizer used the M3-PALS method to give the estimated surface charge. All measurements were performed at 25 °C, with an applied electrical field (E) of 4.9 ± 0.1 V.

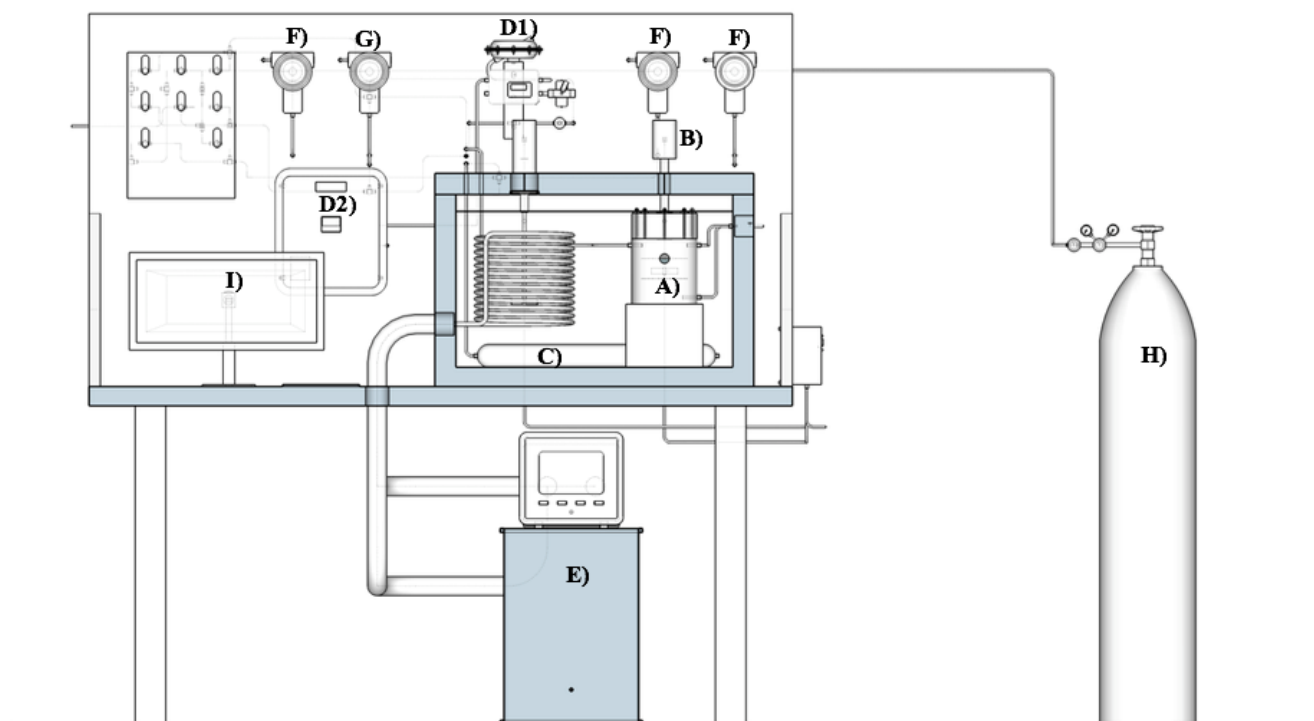


Figure 3: Schematic of the methane hydrate kinetic growth experimental setup. A) stainless steel reactor, B) PPI Dyna/Mag mixer, C) methane gas reservoir, D1) control valve, D2) control box, E) Neslab RTE-740 chiller, F) Rosemount pressure transducers, G) differential pressure transducer, H) methane gas supply tank, I) computer monitor.

Methane hydrate growth experiments

Setup

The experimental setup, used for methane hydrate growth kinetic studies, has previously been used by Bergeron wherein the details of the setup can be found.^{32,33} A schematic of the experimental setup is presented in Figure 3. The hydrate experiments were conducted inside of a 316 stainless steel reactor with a capacity of 600 cm³ and a pressure rating of 12MPa. A PPI Dyna/Mag mixer is mounted on top of the reactor to allow for adequate mixing. Methane gas is supplied to the reactor from a 1000 cm³ reservoir using a control valve in order to maintain a constant pressure throughout the hydrate formation experiment. Both the reactor and the reservoir are placed inside of a 20% ethylene glycol/water mixture to maintain a constant temperature. The temperature of the cooling bath is controlled using a Neslab RTE-740 chiller which maintains the reactor at its operating temperature. The temperature of the reactor is measured using a resistance temperature device probe. The probe used has an accuracy of $\pm 0.15\text{K}$. The pressure of the reactor is monitored using a Rosemount pressure transducer. These transducers are calibrated for a span of 0-14 MPa with an accuracy of $\pm 0.065\%$. A differential pressure transducer is also used and configured to a span of 0-2 MPa with an accuracy of 0.065%. The use of a differential pressure transducer with a smaller range allows for an increased accuracy in the results obtained. A National Instruments data acquisition system is also used with LabVIEW in order to record all the readings.

Procedure

A 700 ppm mixture of the desired KHI block copolymer, dissolved in deionized water, is prepared. The experimental reactor is first

rinsed with the prepared solution to remove any residuals from previous experiments. Once the reactor is rinsed, 300 mL of the experimental solution is injected into the reactor. The pressure of the reactor is then increased to 1000 kPa using methane gas and stirred for several minutes. The pressure of the reactor is then reduced to 100. This purging step is repeat 10-15 times to ensure all air that might have entered the reactor during the loading step of the solution has been removed. After the completion of the final purge cycle, the reactor is left to equilibrate overnight without stirring to get the operating temperature of 277.15K inside of the reactor.

After equilibration, the pressure of the reactor is brought up to the operating pressure of 4735 kPa to be above the thermodynamic equilibrium line and have a driving force of 4 °C favouring the formation of hydrates. The pressure of the reactor reservoir was also increased to 1000 kPa above the operating pressure of the reactor. This was to ensure that enough methane is available to provide the reactor during the experiment to maintain a constant operating pressure. Once the operating temperature and pressure has been achieved, the control valve is activated and the stirrer inside the reactor is turned on at 750 rpm to provide adequate mixing. As hydrates form, the pressure of the methane gas above the liquid reduces as the methane dissolves in the water. Additional methane is fed to the reactor from the reactor reservoir through the control valve to maintain a constant pressure. Once hydrate formation has begun, they are allowed to grow for 1000s. Once enough data has been collected in order to calculate the initial growth rates, the reactor is depressurized to dissociate the hydrates and another experiment with the same sample solution can then begin.

RESULTS AND DISCUSSION

Polymerization of S and PFS to form 1-PS and 1-PPFS macro chain-transfer agent

The first step involved the preparation of the hydrophobic segments of PS and PFS, to be used as macroinitiators for the hydrophilic PVA and PVP blocks. The activity of the chain ends has to be ensured to transfer from one segment to the second segment. The underlying assumption that radicals, during the polymerization, are involved solely in chain growth processes with reversible termination or chain transfer, gives a linear relation of M_n versus conversion, which is a hallmark of truly living polymerizations. The macro-RAFT agents were synthesized with the 2-cyanopropan-2-yl N-methyl-N-(pyridin-4-yl)dithiocarbamate switchable RAFT agent to form 1-PS and 1-PPFS macro chain-transfer agents.

Figure 4 illustrates the kinetics of the polymerization via the semi-logarithmic and linear scale kinetic plots. Figure 4A shows a straight line when the first order growth kinetic model is linearized. While dispersities (\bar{D}) measured for these polymers were relatively high compared to other RAFT polymerizations, similarly high \bar{D} have been observed by other groups when using this switchable RAFT agent.²⁷

From Figure 4C, a linear progression of molecular weight with conversion is observed from the macro chain-transfer at low conversions. At higher conversions (above 40%-45%), however, deviation from linearity is observed, indicating irreversible termination or chain transfer reactions. RAFT synthesis, in general, is governed by its main equilibrium step where an adduct radical intermediate is formed and controls the propagation step. It is desirable to stop reactions before these deviations occur in

order to synthesize polymers with active chain ends and predictably controlled molecular weight and low \bar{D} . With higher conversions and increasing side and termination reactions, an increase in \bar{D} of the synthesized macro chain-transfer agents is seen in Figure 4B.

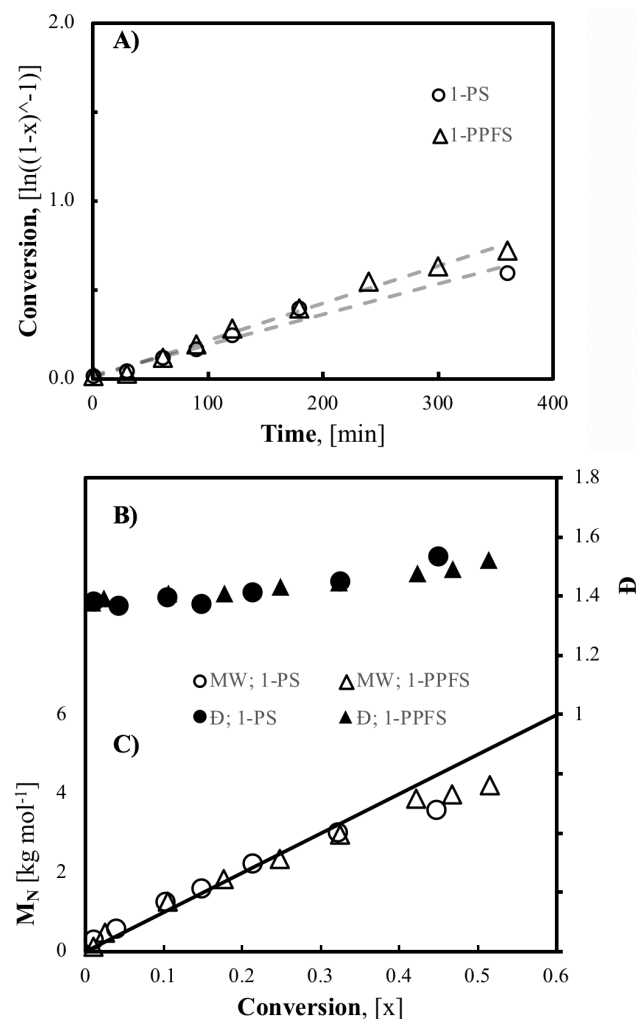


Figure 4: A) Plots of the linearized conversion ($-\ln[1 - X]^{-1}$) (X = conversion) versus time at 70 °C; B) the dispersity (\bar{D}) versus conversion (X); C) the number average molecular weight (M_N) versus conversion (X) for the polymerization of styrene or 2,3,4,5,6-pentafluoro styrene using the switchable RAFT agent to form 1-PS and 1-PPFS macro chain-transfer agents.

The RAFT main-equilibrium reaction can be drawn forward to favour the formation of the RAFT radical intermediate, which controls

the reaction and allows for narrow molecular weight distributions, by increasing the initiator concentration or decreasing the concentration of the RAFT agent. This initiator to RAFT agent concentration ratio has been proposed as a method to obtain narrower molecular weight distributions. A larger than usual ratio has shown to decrease \bar{D} down to 1.1-1.3.^{27,34} Initiator to RAFT agent ratio of 1:20 and 1:15 were first used, however, those polymers obtained had higher dispersities. Increasing the initiator to RAFT agent ratio to 1:5 showed lower dispersities and those ratios have been used for the results in this paper. For the chain extension steps, the ratio was further increased to 1:2.

While lower \bar{D} is widely thought to be desirable for many applications (although this assumption is being challenged³⁵), it should be sufficiently controlled to observe the effect on gas hydrate inhibition as a function of different molecular weights.

Chain extension of 1-PS and 1-PPFS with VAc and VP

1-PS macro chain-transfer agents (CTA) with molecular weights of 4.2 kg mol⁻¹ and 2.2 kg mol⁻¹ (\bar{D} of 1.38 and 1.41) were chain extended with VAc and VP, respectively. Similarly, 1-PPFS macro chain-transfer agents with molecular weights of 4.8 kg/mol and 2.6 kg/mol (\bar{D} of 1.35 and 1.42) initiated the chain extensions of VAc and VP, respectively. From the polymerization kinetic data presented in Figure 5A, the apparent rate constant for the chain extension experiment of PS-PVP, PPFS-PVP, PS-PVAc and PPFS-PVAc were $6.21 \times 10^{-3} \text{ min}^{-1}$, $3.38 \times 10^{-3} \text{ min}^{-1}$, $0.78 \times 10^{-3} \text{ min}^{-1}$ and $1.30 \times 10^{-3} \text{ min}^{-1}$, respectively. A similar apparent rate constant has been observed by Benaglia et al. when chain extending PS with PVAc of with an apparent rate constant of $0.50 \times 10^{-3} \text{ min}^{-1}$ ²⁷ compared to $0.78 \times 10^{-3} \text{ min}^{-1}$ at the same

temperature from this study. The concentrations of the monomers in this study were higher than the ones from Benaglia et al. but the initiator to RAFT agent ratios were the same.

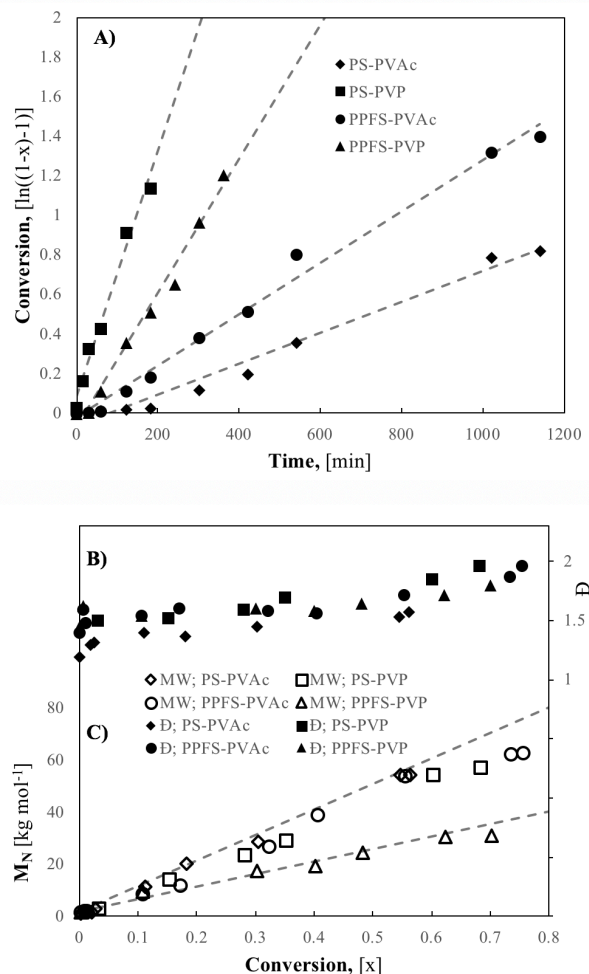


Figure 5: A) Plots of the linearized conversion ($\ln[1 - X]^{-1}$) (X = conversion) versus time at 70 °C; B) the dispersity (\bar{D}) versus conversion (X); C) the number average molecular weight (M_N) versus conversion (X) for the chain extension reactions of PVAc or PVP with 1-PS or 1-PPFS macro chain-transfer agents. At a conversion of 0, the M_n ranges from 2 kg mol⁻¹ to 4 kg mol⁻¹ depending on the macroinitiator.

It was observed that the polymerization rate of the chain extension with PVAc was lower than PVP for both 1-PS and 1-PPFS macro chain-transfer agents. With PVAc, the 1-PPFS macro chain-transfer agent exhibited a

faster growth rate than the 1-PS macro chain-transfer agent. The differences in polymerization rate are not solely due to the propagation rate constant, k_p , as k_p for bulk Vac³⁶ is about an order of magnitude higher than that of VP³⁷ at 70°C, based on pulsed-laser polymerization/size exclusion chromatography (PLP-SEC) measurements suggesting that the propagation rate constants are not the sole drivers for polymerization rate in these chain extensions ($k_{p,VAc} \sim 1.0\text{--}1.3 \times 10^4 \text{ L mol}^{-1} \text{ s}^{-1}$ versus $k_{p,VP} \sim 2.9 \times 10^3 \text{ L mol}^{-1} \text{ s}^{-1}$).^{36,37} There may be differences due to concentration of monomer and macroinitiator in each system as well as the effect of the chain end on the RAFT agent.

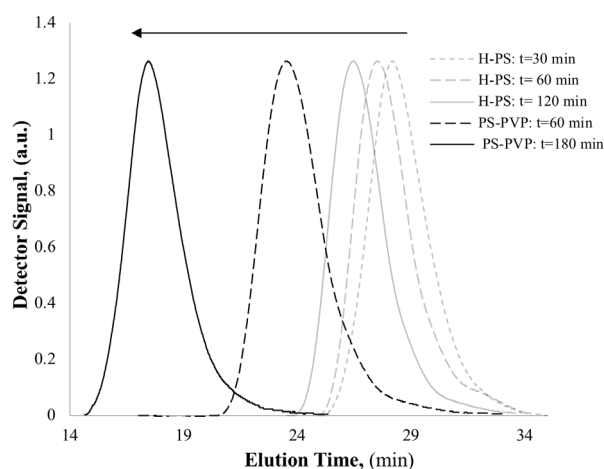


Figure 6: GPC chromatograms (molecular weight distributions, MWDs) for characteristic synthesis of 1-PS macro chain-transfer agent followed by its subsequent chain extension with PVP to form block copolymer PS-PVP. H-PS indicates the homopolymer macro-CTA.

When chain extending to form the PVP segment of the block copolymer, a faster propagation rate with 1-PS was achieved compared to that using 1-PPFS. In a comprehensive review by Destarac, the choice of the R-group on the RAFT agent was shown to have a significant effect on the rate constant of polymerization.³⁸ With a 2-cyanopropyl R-group, as is the case in this

study as well, a more electrophilic radical, such as the 2,3,4,5,6-pentafluorostyrene, add very rapidly and show higher rate constants.³⁹

In terms of the success of chain extension, Figure 6 shows the molecular weight distributions for the 1-PS macro chain-transfer agent as well as the molecular weight distributions for its chain extended product with PVP to form a PS-PVP block copolymer. The distributions are monomodal, indicative of a successful polymerization and chain extension. It illustrates the active feature of the synthesized macro chain-transfer agent with the switchable RAFT agent. Similar clean chain transfers were observed for the PS-PVAc chain extensions.

While not presented in this paper as they were not used for methane hydrate inhibition, both PVAc and PVP chain extensions were able to form block copolymers of up to 300 kg mol^{-1} to 400 kg mol^{-1} with dispersities ranging from 1.6 to 1.9. Dispersities further increased at higher monomer conversions going up to 2.5 at 90% conversions. Similarly, deviations from linearity in M_N vs conversion are observed at higher conversions as more undesired termination reactions occur.

Hydrolysis

The block copolymers containing poly(vinyl acetate) were hydrolyzed in order to form poly(vinyl alcohol) to allow the block copolymer to be water-soluble. The copolymer was dissolved in benzene at 70 °C to which sodium hydroxide was added for selective hydrolysis. The hydrolysis reaction was conducted for 7 hours with mixing until the ¹H-NMR showed no acetyl groups remaining. The ¹H NMR spectra before and after hydrolysis are shown in Figure 2. The aromatic protons for styrene were observed at $\delta = 6.2\text{--}7.4 \text{ ppm}$, while the vinylic protons

were at $\delta = 4.6\text{--}5.2$ ppm. For VAc-containing copolymers, after hydrolysis, the acetylic protons ($\delta = 1.9\text{--}2.1$ ppm) disappeared while hydroxyl peaks ($\delta = 4.5\text{--}4.6$ ppm) appeared.

Critical micelle concentration measurements

The critical micelle concentrations (CMC) of the synthesized block copolymers were measured. Knowing the extent to which these KHIs have micellized in solution can help us better understand their effect on hydrate inhibition. Above the CMC, all polymers in solutions micellize. As CMCs vary widely with different amphiphilic block copolymer structures, it becomes important to measure this concentration to know how far, relative to the CMC, the concentration of KHI in solution is. If the polymer concentration in solution during hydrate inhibition is below the CMC, the polymers should be located at the interface between the gas and clathrate cage. Above the CMC, all amphiphilic block polymers in solution will micellize. While there are other methods for determining the CMC of a polymer, such as measuring the surface potential,^{40,41} through density and viscosity,⁴¹ and light scattering,⁴² there are several challenges towards applying them in different conditions.⁴³ Measuring the zeta surface potential is also a viable method to calculating the CMCs. This method has previously been used to measure the CMC of colloidal suspensions of vitamins and various salts.⁴⁴ More recently, this method has been effective in measuring the CMC of larger molecules.³⁰ We applied this method to determine the CMC of polymeric macrosurfactants (identified in Table 2) for KHIs. Figure 7 illustrates the dependence of the magnitudes of the measured signals from the ZetaSizer on the concentrations of the

synthesized block copolymer. In aqueous solutions of amphiphilic block copolymers, the hydrophobic end groups tend to agglomerate together as they repel from the water around them.⁷

At low concentrations of block copolymers, these surfactants tend to adhere to the water-air interface. With increasing concentrations, these surfactants dissolve in the water and remain mostly well suspended as there are a low number of surrounding amphiphilic block copolymers to agglomerate with. While the polymers are suspended in solution, the zeta potential is higher due to the presence of the hydrophobic groups in the polymer. As the concentration of block copolymers in water increases, the hydrophobic end groups of the ABCs find surrounding hydrophobic groups and agglomerate. Beyond a “critical” concentration of ABCs in water, when the water-air surface is also saturated, all surfactants added aggregate in the bulk solution and form micelles.⁴⁵ As micelles form, the hydrophobic ends get hidden under the hydrophilic groups, and effectively lower the zeta potential. This zeta potential keep decreasing until the CMC. This behaviour is seen in Figure 7, where a decrease in surface potential is observed with increasing concentration of block copolymers due to a large hydrophilic end of the polymers. The surface potential, beyond the CMC, is seen to be constant and at its minimal value. By measuring the zeta potential, we can determine that concentration and which the zeta potential is lowest and stop reducing further, as this will be the CMC. The CMC is located at the intersection of the two distinct portions (illustrated as the intersection of the two dotted linearized trendlines).

Table 2: Identification of the block copolymers synthesized for determination of critical micelle concentration (CMC).

Experiment ID ^a	Overall MW (M _n , kg mol ⁻¹)	Mole fraction of macro CTA in polymer [PS or PPFS]	Đ	MW of macro CTA in polymer ^b [PS or PPFS] (M _n , kg mol ⁻¹)	CMC (x10 ⁻⁴ M)
PS-PVA-40(0.05)	42.8	0.06	1.44	4.2	2.0
PPFS-PVA-40(0.05)	44.1	0.04	1.50	4.8	1.5
PS-PVP-20(0.1)	21.6	0.11	1.51	2.2	5.0
PPFS-PVP-20(0.1)	23.1	0.09	1.55	2.6	4.5

^a The experiment ID indicates the hydrophilic and hydrophobic monomers present in the block copolymer. The ID term AA-BB-11(0.0) is used to describe block copolymers where AA is the hydrophobic cap of the polymer (PS or PPFS), BB is the hydrophilic chain (PVA or PVP), 11 is the overall molecular weight, and (0.0) is the mole fraction of the hydrophobic monomer in the copolymer as measured by H-NMR.

^b The number average molecular weight of the macro chain-transfer agent used for the chain extension.

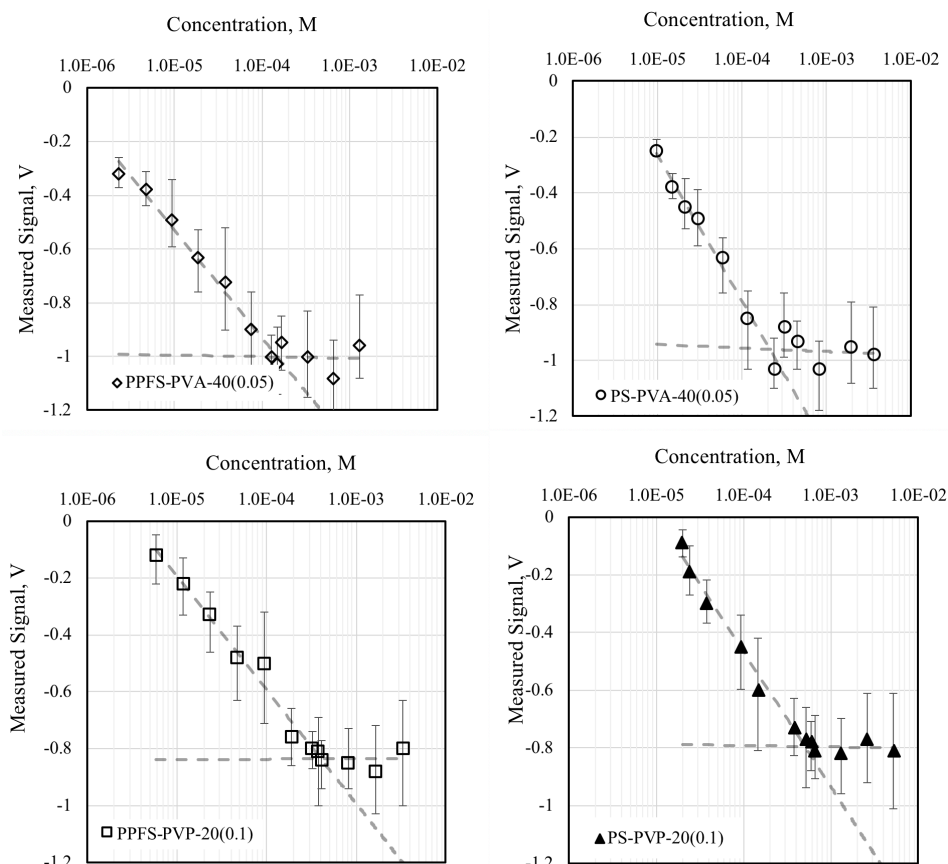


Figure 7: Dependence of the magnitudes of measured signals on the concentrations of synthesized amphiphilic block co-polymers. The CMC is located at the intersect of the two distinct sections of the measured signal (illustrated as the intersection of the two dotted linearized trendlines).

The CMCs of the block copolymers with a lower overall molecular weight was calculated to be significantly higher than CMCs of block copolymers with a higher overall molecular weight. Block copolymers with a higher CMC would allow higher concentrations of these polymers in solution while retaining their hydrophobic area of effect in solution. This has an impact on hydrate inhibition as the hydrates grow at the water/gas interface. It is desirable for block copolymer inhibitors to be at this interface rather than to be completely micellized. For block copolymers with the same molecular weight, those with a more hydrophobic end group (e.g. PPFS instead of PS) exhibited a lower CMC than those with PS as the hydrophobic end group. These trends have been observed by others using different

polymers and other CMC measurement methods.^{46,47}

In a study by Yoshida investigating the micellization of poly(vinyl phenol)-*block*-poly(styrene), they concluded that the poly(styrene) block chain length had a lesser effect on the CMC than the chain length of the hydrophilic chain.⁴⁸ In a more recent study, the micellization of poly(styrene)-*block*-poly(glycidol) was studied. The CMC of those block copolymers, with similar molar ratio of hydrophile to hydrophobe than this study, was reported to be 4×10^{-4} M.⁴⁹ Another study with poly(styrene)-*block*-poly(ethylene oxide) at higher molecular weights (16.2 kg mol^{-1}) measured the CMC to be 55×10^{-4} M.⁵⁰ As expected, the block copolymers in this study exhibit lower CMCs due to their molecular weight being up to 2.5

times higher. Khan and Siddiq, for instance, tested the effect of end group hydrophobicity on its CMC and observed a decrease in CMC with increasing hydrophobicity due to enhanced association ability of the polymer allowing micellization to occur at lower concentration.⁵¹ The comparable results between this study and previously studied CMCs of block copolymers suggest this method of measuring the CMC, using the surface charge measurement, is a viable method for amphiphilic block copolymers of higher molecular weight.

Methane Hydrate Growth

Figure 8, shown below, illustrates a typical curve obtained during a hydrate growth experiment. Methane gas first begins to dissolve in the sample solution within the reactor which allows for the nucleation step to occur. This nucleation process is stochastic and yet to be fully understood. In this process, hydrate cages and clumps of particles grow and decompose until they reach a thermodynamically stable, critical nucleus, size.⁵² After the hydrate crystals have reached a critical nucleus size, crystal growth can occur. This hydrate crystal growth phase is indicated by an increase in methane consumption. The growth phase is linear and is also corroborated with a slight increase in temperature (not shown in the figure) occurring due to the crystal growth phase being exothermic.⁵³

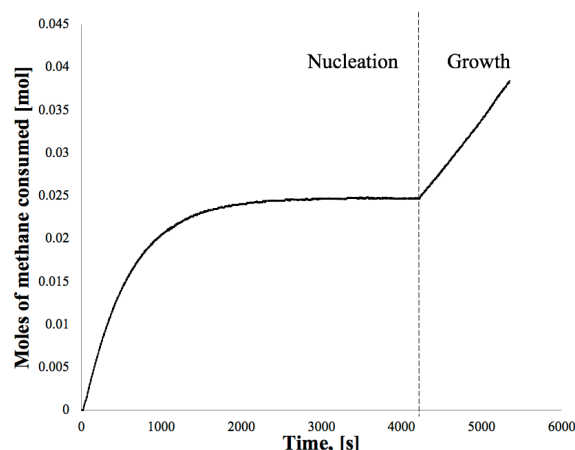


Figure 8: Typical curve obtained during hydrate growth experiments.

The highest methane consumption rates were observed for pure methane-water hydrate systems, where no KHIs were present, with a consumption rate of $1.142 \times 10^{-5} \text{ mol s}^{-1}$, as shown in Figure 9. The addition of PVP-40, a commercially available and commonly used KHI^{54,55} resulted in a drastic, and expected, reduction of the consumption rate of methane, by 50%. The addition of PVA as a KHI to the pure methane-water system also resulted in a reduction of methane consumption, however, not as drastically as PVP, at 30%. PVA and PVP both have a hydrophobic vinyl backbone, but PVA has a more hydrophilic $-\text{OH}$ group as opposed to the lactam group present in PVP. Due to the very strong hydrophilicity of $-\text{OH}$, PVA is very good at remaining soluble in water as well as adsorbing onto to hydrophilic crystal growth front of hydrates. However, the significantly smaller size of PVA compared to PVP can explain the reduced inhibition of methane hydrates, since less surface is covered, despite having more pronounced amphiphilic properties.

The addition of PS, a hydrophobic end group, to the PVA homopolymer, in order to form a PVA-PS block copolymer, resulted in a further improved inhibition. The PVA-PS block copolymer inhibited methane hydrate formation and reduced the methane

consumption rate by 49%, very close to the rate of PVP. By substituting the PS with a more hydrophobic PPFs end group, the PVA-PPFS block copolymer exhibited a higher inhibition of methane hydrate formation, exhibiting a methane consumption rate 77% lower than a pure methane-water

system with no KHI. This KHI resulted in 27% greater inhibition than the PVP homopolymer currently being used by the industry.⁵⁴

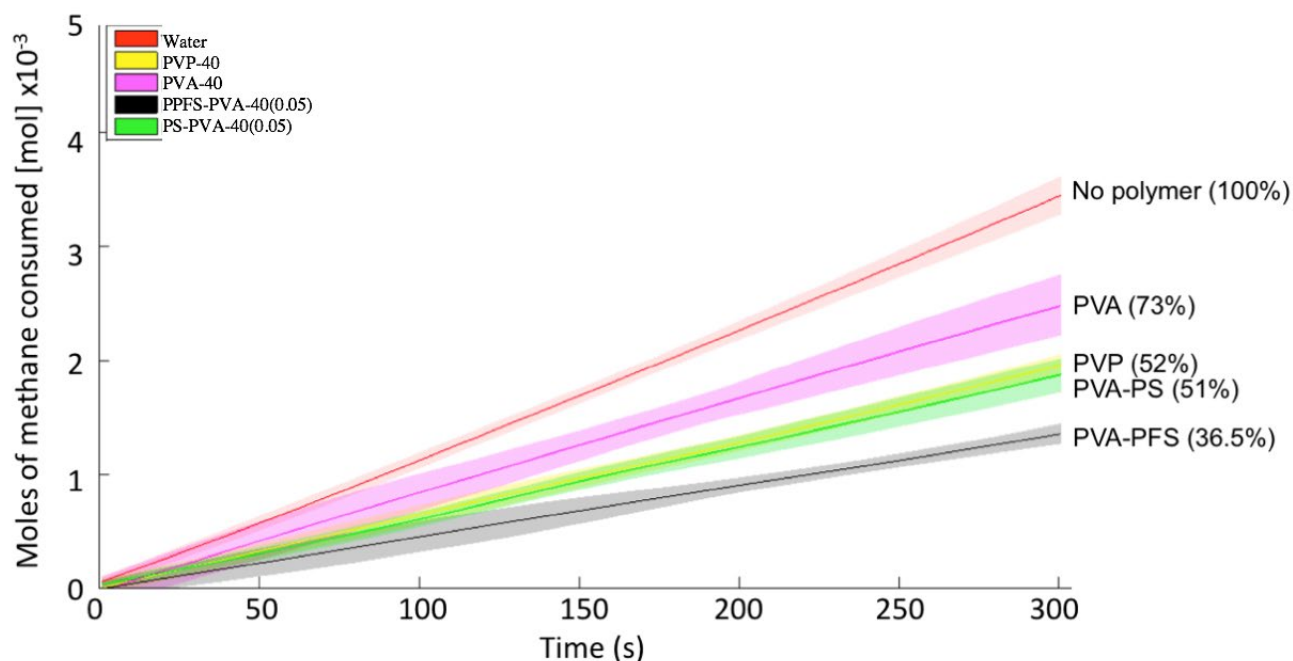


Figure 9: Methane gas hydrate mole consumptions observed with various kinetic hydrate inhibitor polymers. Experimental temperature conditions are 275.2 K. All experiments are under a constant 4°C driving force. The shaded parts represent the 95% confidence interval. The moles of methane consumed with the presence of PS-PVA (green line) and PPFs-PVA (black line) block copolymers are compared with a PVA homopolymer (magenta line), and a commercially available PVP homopolymer (yellow line). Methane consumption in pure water is also shown (red line).

Table 3: Methane gas consumption rates obtained from hydrate growth experiments of PVP, PVA, and PVA-block copolymers.

Experiment ID	Methane consumption rate ($\times 10^{-5} \text{ mol s}^{-1}$)
Water	1.142
PVP-40	0.571
PVA-40	0.801
PS-PVA-40(0.05)	0.583
PPFS-PVA-40(0.05)	0.263

Similar experiments were conducted using PS-PVP and PPFs-PVP block copolymers to observe the effect of end group hydrophobicity of the KHI on its inhibition

potential. The PVP homopolymer, at a lower molecular weight of $20\,000 \text{ g mol}^{-1}$, showed a similar consumption rate than the PVP homopolymer at $40\,000 \text{ g mol}^{-1}$. As expected, this further verified that the effect of molecular weight of PVP in that range is negligible.

By adding a hydrophobic cap to the PVP homopolymer, a similar trend, as previously, was seen where the methane consumption rate further decreases. Using PS-PVP block copolymer, increased inhibition compared to PVP homopolymer was seen, as shown by a 20% additional reduction of methane consumption rate during the growth phase

compared to the PVP homopolymer. After substituting the PS end group with a more hydrophobic PPFS end group, the consumption rate of methane for PVP-PPFS

further decreased by 35% compared to that of PVP-PS block copolymer.

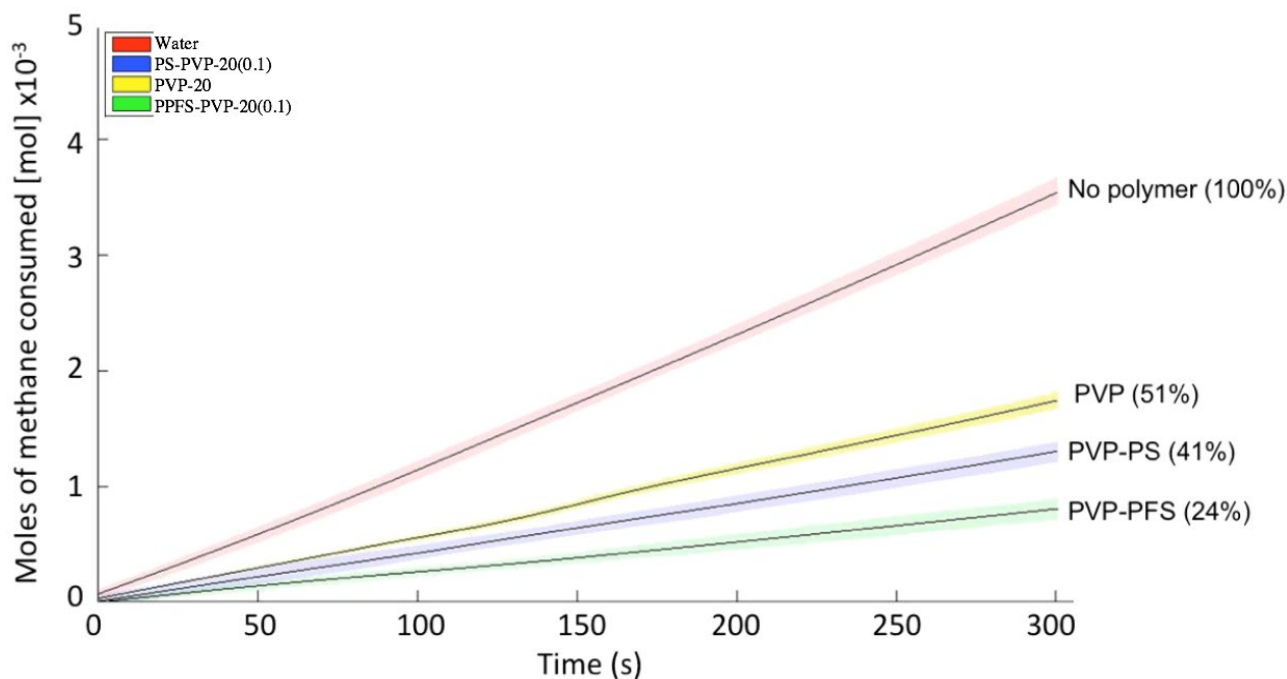


Figure 10: Methane gas hydrate mole consumptions observed with various kinetic hydrate inhibitor polymers. Experimental temperature conditions are 275.2 K. All experiments are under a constant 4 degrees Celsius driving force. The shaded part represents the 95% confidence interval. The moles of methane consumed with the presence of PS-PVP (blue line) and PPFS-PVP (green line) block copolymers are compared with a PVP homopolymer (yellow line). Methane consumption in pure water is also shown (red line).

Table 4: Methane gas consumption rates obtained from hydrate growth experiments of PVP, and PVP-block copolymers.

Experiment ID	Methane consumption rate ($\times 10^{-5} \text{ mol s}^{-1}$)
Water	1.142
PVP-20	0.569
PS-PVP-20(0.1)	0.345
PPFS-PVP-20(0.1)	0.217

This two to three-fold reduction in methane consumption rate is significant due to the small concentrations of KHI used. The KHI concentrations in solution are much lower than their respective CMC. While micelles still form in solution, most of the KHI chains

are not in that structure. At much higher concentrations of KHI in solution, Posteraro had seen that further increasing concentrations of KHI (PVP) in solution did not substantially increase hydrate inhibition.⁵⁶

Near the hydrate-liquid interface, the attraction of block copolymer toward the surface of the growing hydrate crystal is dependent on the entropic attraction parameter U^e which reflects the entropic interactions between polymers and surfaces.^{57,58} With an increase in the strength of attraction, or with a decrease in temperature, polymer may adsorb onto the crystal surface.⁵⁹ With large values of

attraction, the polymer has been seen to adsorb onto the surface in a pancake-like conformation covering a large area. With lower attraction, however, the polymer adopts a mushroom like conformation, coming in contact with a smaller area on the surface.^{60,61} While this entropic attraction parameter, U^e , is difficult to obtain, it can be estimated using the Flory-Huggins χ parameter of interaction.⁵⁸ When the polymer is in a good solvent, the χ parameter of interaction tends to be low and the polymer tends to expand. Conversely, if the polymer is in a bad solvent, the χ parameter of interaction tends to be higher and the polymer tends to collapse and cluster together, decreasing the surface area covered when adsorbed on the crystal surface.^{62,63}

These χ parameter of interaction can be calculated using:

$$\chi = \frac{V_m}{RT} (\delta_A - \delta_B)^2 + 0.34$$

where V_m is the molar volume, δ_A and δ_B are the Hildebrand solubility parameters of the solvent and the polymer, respectively. The solubility parameters can be found in literature or, for more complex polymer structures such as PVP and PPFS, estimated using the Bowden and Jones method to account for the contribution of each group present in the polymer to its solubility parameter.⁶⁴ Table 5 presents the solubility

parameters used to calculate the χ parameter of interaction.

Table 6 presents the χ parameters of interaction calculated for the polymers in our system. While these values are high, indicating that they tend to not be easily soluble in the solvents, a trend is seen where the more hydrophilic polymers have a few fold lower χ parameters in water than the hydrophobic polymers.

This indicates that these polymers would be more swollen in water and when adsorbing onto the crystal surface, form a pancake-like structure and cover a larger surface area. Similarly, with methane, the more hydrophobic polymers show a few-fold lower χ parameter than the hydrophilic polymer. These hydrophobic polymers increase their tendency to attract the dissolved methane present in the liquid and inhibit hydrate growth more effectively.

Table 5: Solubility parameters used for the calculation of χ parameters of interaction.

	Solvent		Polymer			
	H ₂ O ^a	CH ₄ ^b	PVA ^a	PVP ^c	PS ^a	PPFS ^d
δ ($\times 10^5 \text{ MPa}^{1/2}$)	1.52	0.42	0.96	0.77	0.59	0.47

a) Value obtained from the CRC Handbook of Solubility Parameters and Other Cohesion Parameters.⁶⁵ b) Value obtained from Prausnitz & Shair.⁶⁶ c) Value obtained from Lu *et al.*⁶⁷ d) Value estimated using Bowden and Jones method.⁶⁴

Table 6: interaction parameters calculated for the polymers in solvents.

Solvent	Polymer:	PVA	PVP	PS	PPFS
H ₂ O		2.40	4.39	16.76	18.51
CH ₄		28.4×10^2	11.5×10^2	2.6×10^2	0.24×10^2

The block copolymer of PVA with a strong hydrophobic PPFS polymer is seen to inhibit hydrate growth more than the block copolymer with the less hydrophobic PS. The same trend is seen in the inhibition potential of the block copolymer of PVP with PS and PPFS where the block copolymer of the more hydrophobic PPFS inhibits hydrate growth more than PS, correlating with the trend seen in the χ parameters of interaction. It is important to stress that this is a correlation, and not the only cause of the trends seen with hydrate inhibition. Other variables such as polymer structure and confirmation in solution may also play a role, but further testing need be done to confirm.

CONCLUSIONS

This paper reports the successful synthesis of amphiphilic block copolymers of poly(styrene) or poly(2,3,4,5,6-pentafluorostyrene) as the hydrophobic segment with poly(vinyl acetate) or poly(vinyl pyrrolidone) water-soluble segments using the 2-cyanopropan-2-yl N-methyl-N-(pyridin-4-yl)dithiocarbamate switchable RAFT agent. PS or PPFS were first synthesized to form macro chain-transfer agents (CTA) with control of the molecular weight distribution. These macro-CTAs were then successfully chain extended with VAc or VP to form macromolecular surfactants.

This paper also presents zeta surface potential measurements as a method to determining the CMC of amphiphilic block copolymers with high molecular weights. Block copolymers with lower overall molecular weights exhibited higher CMCs

than polymers with higher molecular weights. For block copolymers with the same molecular weight, those with a more hydrophobic end exhibited a lower CMC than those with a lesser hydrophobic end group.

The successful synthesis of LAM-MAM block copolymers using a switchable RAFT agent allows for the engineering of amphiphilic block copolymers with specific characteristics that can impact their use, among others, as kinetic hydrate inhibitors. This marks one of the first times that controlled radical polymerization has been targeted to design KHIs based on block copolymer motifs.

The addition of PVA as a KHI to the pure methane-water system resulted in a 30% reduction of methane consumption during the growth phase compared to that of the pure methane-water system with no KHIs. The addition of PS, a hydrophobic end group, to the PVA homopolymer, in the form of a PVA-PS block copolymer, further decreased methane consumption during growth, at 49% compared to the pure methane-water system with no KHIs. By substituting the PS with a more hydrophobic PPFS end group, the methane hydrate growth rate further decreased by 27%. This PVA-PPFS inhibitor resulted in greater inhibition than the PVP homopolymer.

Similar trends were observed when looking at PVP based copolymer with more pronounced hydrophobic properties. The addition of a hydrophobic PS end group to the PVP polymer resulted in an increased

inhibition shown by a 20% reduction of methane consumption rate during the growth phase compared to the methane-water system with a PVP homopolymer inhibitor. This PS end group was substituted by a more hydrophobic PPFS end group and the consumption rate of methane for PVP-PPFS further decreased by 35% compared to that of PVP-PS. The trends seen, where the block copolymer of the more hydrophobic PPFS inhibits hydrate growth more than PS for both PVA and PVP, correlates with the trends seen in the Flory-Huggins χ parameters of interaction calculated for these polymers. These results further emphasize the role of the structure of the KHI and its amphiphilic properties in its inhibition potential. Determining the effect of certain variables on the inhibition potential of gas hydrates is crucial as this information can be used to improve the kinetic inhibitors currently used industrially to increase their efficiency. The results from these alternative KHI designs can either improve current KHIs used industrially or lead to new KHIs to safely handle gas hydrates in situations where their formation is thermodynamically favourable.

ACKNOWLEDGEMENTS

The authors would like to thank the Natural Sciences and Engineering Research Council of Canada (NSERC), McGill University, as well as the McGill Engineering Doctoral Award (MEDA), Bourse the Doctorat en Genie Hydro Quebec, Vadasz Fellowship, and the Fonds Quebecois de la Recherche sur la Nature et les Technologies (FQRNT) for their financial support and funding.

REFERENCES

1. Clathrate Hydrates of Natural Gases: Third Edition; E. D. Sloan and C. A. Koh; Taylor and Francis Group, **2008**.
2. E. G. Hammerschmidt, *Ind. Eng. Chem.* **1934**, 26, 851–855.
3. T. J. Crone, and M. Tolstoy, *Science*, **2010**, 330, 6004–6034.
4. F. E. Anderson, and J. M. Prausnitz, *AIChE J.*, **1986**, 32, 1321–1333.
5. C. A. Koh, *Chem. Soc. Rev.* **2002**, 31, 157–167.
6. R. Larsen, C. A. Knight, and E. D. Sloan, *Fluid Phase Equilib.* **1998**, 353–360.
7. A. Perrin, O. M. Musa, and J. W. Steed, *Chem. Soc. Rev.* **2013**, 42, 1996–2015.
8. B. J. Anderson, J. W. Tester, G. P. Borghi, and B. L. Trout, *J. Am. Chem. Soc.* **2005**, 127, 17852–17862.
9. H. Zeng, V. K. Walker, and J. A. Ripmeester, *Angew. Chemie Int. Ed.* **2007**, 46, 5402–5404.
10. E. D. Sloan, *Energy and Fuels* **1998**, 12, 191–196.
11. H. E. King, J. L. Hutter, M. Y. Lin, and T. Sun, *J. Chem. Phys.* **2000**, 112.
12. Y. Mai, A. Eisenberg, R. J. M. Nolte, J. V. M. van Hest, S. P. Armes, A. J. Ryan, A. L. Lewis, G. Battaglia, S. Tan, A. Brisson, V. Dupuis, O. Sandre, and S. Lecommandoux, *Chem. Soc. Rev.* **2012**, 41, 5969.
13. G. Moad, E. Rizzardo, and S. H. Thang, *Aust. J. Chem.* **2009**, 62.
14. F. T. Reyes, M. A. Kelland, N. Kumar, and L. Jia, *Energy & Fuels* **2015**, 29, 695–701.
15. L. Ree, M. A. Kelland, D. Haddleton, and F. Alsubaie, *Energy & Fuels* **2017**, 31, 1355–1361.
16. M. Szwarc, M. Levy, and R. Milkovich, *R. J. Am. Chem. Soc.* **1956**, 78, 2656–2657.
17. W. O. Webster, W. R. Hertler, D. Y. Sogah, W. B. Farnham, and T. V. RajanBabu, *J. Am. Chem. Soc.* **1983**, 105, 5706–5708.
18. A. F. Halasa, *Rubber Chem. Technol.* **1981**, 54, 627–640.
19. The chemistry of radical polymerization; G. Moad, D. H. Solomon; Elsevier, **2006**.
20. Principles of polymerization; G. G. Odian; Wiley, **2004**.
21. G. Moad, E. Rizzardo, and S. H. Thang, *Aust. J. Chem.* **2012**, 65, 985.
22. M. K. Georges, R. P. N. Veregin, G. K. Hamer, and P. M. Kazmaier, *Macromol.*

- Symp.* **1994**, 88, 89–103.
23. Radicals in Organic Synthesis; M. Georges; Wiley-VCH Verlag GmbH, **2001**, chapter 24, 479–488.
 24. Handbook of RAFT Polymerization; E. Rizzardo, G. Moad, S. H. Thang; Wiley-VCH Verlag GmbH & Co. KGaA, **2008**, 189–234.
 25. J. Chiefari, Y. K. Chong, F. Ercole, J. Krstina, J. Jeffery, T.P.T. Le, R.T.A. Mayadunne, G.F. Meijs, C.L. Moad, G. Moad, E. Rizzardo, and S.H. Thang, *Macromolecules*, **1998**, 31, 5559–5562.
 26. G. Moad, E. Rizzardo, and S. H. Thang, *Polymer*, **2008**, 49, 1079–1131.
 27. M. Benaglia, M. Chen, Y. K. Chong, G. Moad, E. Rizzardo, and S. H. Thang, *Macromolecules* **2009**, 42, 9384–9386.
 28. E. Biccocchi, Y. K. Chong, L. Giorgini, G. Moad, E. Rizzardo, and S. H. Thang *Macromol. Chem. Phys*, **2010**, 211, 529–538.
 29. M. Benaglia, J. Chiefari, Y. K. Chong, G. Moad, E. Rizzardo, S. H. Thang, *J. Am. Chem. Soc.* **2009**, 131, 6914–6915.
 30. Y. Song, R. Sun, K. Zhao, X. Pan, H. Zhou, and D. Li, *Colloid Polym. Sci.* **2015**, 293, 1525–1534.
 31. Fluorescence Studies of Polymer Containing Systems; M. Karayianni, and S. Pispas; Springer Verlag, **2016**.
 32. S. Bergeron, and P. Servio, *AIChE J.* **2008**, 54, 2964–2970.
 33. S. Bergeron, and P. Servio, *Fluid Phase Equilib.* **2008**, 265, 30–36.
 34. G. Moad, D. Keddie, C. Guerrero-Sanchez, E. Rizzardo, and S. H. Thang, *Macromol. Symp.* **2015**, 350, 34–42.
 35. M. A. Hillmyer, *J. Polym. Sci. Part B Polym. Phys.* **2007**, 45, 3249–3251.
 36. T. Junkers, D. Voll, and C. Barner-Kowollik, *E-Polymers*, **2009**, 1–8.
 37. M. Stach, I. Lacík, D. Chorvát, M. Buback, P. Hesse, R. A. Hutchinson, and L. Tang, *Macromolecules*, **2008**, 41, 5174–5185.
 38. M. Destarac, *Polym. Rev.*, **2011**, 51, 163–187.
 39. S. Harrisson, X. Liu, J.-N. Ollagnier, O. Coutelier, J.-D. Marty, and M. Destarac *Polymers (Basel)*, **2014**, 6, 1437–1488.
 40. E. Piera, P. Erra, and M. R. Infante, *J. Chromatogr. A* **1997**, 757, 275–280.
 41. M. Bielawska, A. Chodzińska, B. Jańczuk, and A. Zdziennicka, *Colloids and surfaces*, **2013**.
 42. Ö. Topel, B. A. Çakır, L. Budama, and N. Hoda, *J. Mol. Liq.*, **2013**, 177, 40–43.
 43. J. Carpena, P. Aguiar, A. Bernaola-Galván, and C. C. Ruiz, *Langmuir*, **2002**, 18, 6054–6058.
 44. Y. C. Chiu, C. Y. Kuo, and C. W. Wang, *J. Dispers. Sci. Technol.* **2000**, 21, 327–343.
 45. J. B. Grindley, and C. R. Bury, *J. Chem. Soc.*, **1929**, 679–684.
 46. R. Zana, *Adv. Colloid Interface Sci.* **2002**, 97, 205–53.
 47. M. Nakayama, and T. Okano, *Biomacromolecules*, **2005**, 6, 2320–2327.
 48. E. Yoshida, *Polym. J.* **2003**, 35, 965–971.
 49. Ł. Otulakowski, M. Gadzinowski, S. Slomkowski, T. Basinska, A. Forys, A. Dworak, and B. Trzebiecka, *Eur. Polym. J.*, **2018**, 99, 72–79.
 50. F. Ahmad, M. K. Baloch, M. Jamil and Y. J. Jeon, *J. Appl. Polym. Sci.*, **2010**, 118, 1704–1712.
 51. A. Khan, and M. Siddiq, *J. Polym. Res.* **2014**, 21.
 52. P. Englezos, *Ind. Eng. Chem. Res.*, **1993**, 32, 1251–1274.
 53. R. O'Reilly, N. S. Jeong, P. C. Chua, and M. A. Kelland, *Chem. Eng. Sci.* **2011**, 66, 6555–6560.
 54. M. A. Kelland, T. M. Svartaas, J. ØVsthus, and T. A. Namba, *Ann. N. Y. Acad. Sci.* **2000**, 912, 281–293.
 55. S. Xu, S. Fan, Y. Wang, and X. Lang, *J. Chem. Eng. data*, **2015**, 311–318.
 56. D. Posteraro, J. Ivall, M. Maric, and P. Servio, *Chem. Eng. Sci.* **2015**, 126, 91–98.
 57. V. S. Minnikanti, Z. Qian, and L. A. Archer, *J. Chem. Phys.* **2007**, 126.
 58. V. S. Minnikanti, and L. A. Archer, *Macromolecules*, **2006**, 7718–7728.
 59. P. G. De Gennes, *Macromolecules*, **1981**, 14, 1637–1644.
 60. Comprehensive Polymer Science; P. G.

- de Gennes; American Physical Society, **1989**, 1, 1–42.
61. Polymer science : a comprehensive reference; K. Matyjaszewski, and M. Möller; Elsevier, **2012**.
 62. M. L. Huggins, *J. Chem. Phys.* **1941**, 9, 440–440.
 63. F. Rodríguez-Ropero, T. Hajari, and N. F. A. van der Vegt, *J. Phys. Chem. B* **2015**, 119, 15780–15788.
 64. R. F. A. Fedors, *Polym. Eng. Sci.* **1974**, 14, 147–154.
 65. CRC handbook of solubility parameters and other cohesion parameters; A. F. M. Barton; CRC Press, **1991**.
 66. J. M. Prausnitz, and F. H. A. Shair, *AIChE J.* **1961**, 7, 682–687.
 67. L. Li, Z. Jiang, J. Xu, and T. Fang, *J. Appl. Polym. Sci* **2014**, 131.